J. Min. Metall. Sect. B-Metall. 46 (2) B (2010) 171 - 180

Journal of
Mining and
Metallurgy

PRECIPITATION SEQUENCE OF AN AGED Al-Mg-Si ALLOY

X. Fang[*], M. Song[*, #], K. Li[*] and Y. Du[*]

[*]State Key Laboratory of Powder Metallurgy, Central South University,
Changsha 410083, China

(Received 04 Jun 2010; accepted 15 October 2010)

Abstract

Heat treatable Al-Mg-Si alloys can be strengthened via the precipitation of metastable phase particles. The precipitation sequence of an Al-0.89Mg-0.75Si alloy with trace Fe and Zn elements during aging at 180 °C has been investigated by transmission electron microscope (TEM), high resolution transmission electron microscope (HRTEM) and hardness measurements. It has been shown that the precipitation sequence of the alloy can be identified as follows: supersaturated solid solution → G.P. zones → metastable β'' precipitates → metastable β' precipitates → stable β phase + Si particles. It is indicated that β'' phase remains stable up to 30 hours at 180 °C. The hardness measurements during aging realize that the main strengthening phase for the investigated Al-Mg-Si alloy is β'' precipitates and the maximum hardness is obtained after aging at 180 °C for 4~6.5 hours.

Keywords: Al-Mg-Si alloy; Precipitation; Aging; Hardness; Transmission electron microscope.

1. Introduction

Al alloys is one of the most widely used non-ferrous structural materials in industry, and many sub-systems of multi-component Al alloys have been studied, including the establishment of their thermodynamic database [1-2]. The 6000 series Al-Mg-Si alloys are widely used in aerospace and civil industries because of their low densities and a favorable combination of strength and resistance to corrosion. The strength of the alloys can be largely enhanced by T6 artificial aging treatment after solution and

[#] *Corresponding author: min.song.th05@alum.dartmouth.org*

DOI: 10.2298/JMMB1002171F

quenching treatments. During the aging treatment the supersaturation of the solute atoms in aluminum matrix is gradually reduced. The strength is thus increased because a high density of fine coherent or semi-coherent precipitates nucleates and grows. The controlling of the precipitation during artificial aging is critical to obtain optimal mechanical properties of the alloys. A generally accepted precipitation sequence of a solution and quenching treated Al-Mg-Si alloy during artificial aging can generally be described as follows: supersaturated solid solution → G.P. zones → metastable β″ precipitates → metastable β′ precipitates → stable β phase [3-7]. This precipitation sequence was observed for most investigated Al-Mg-Si alloys within a relatively wide temperature range. Previous investigation indicated that equilibrium Si phase is formed at the end of the precipitation sequence if the atomic ratio of Mg to Si is less than 2, and this phase can nucleate along the stable β particles [8]. However, considerable confusions still exist concerning the precipitation process and the compositions of the intermediate precipitates. Some researchers suggested that several other precipitates, such as U1 and B′, might also be formed in addition to the above mentioned precipitates [9-14].

In general, the G.P. zone in Al-Mg-Si alloys was reported to have a spherical shape and be fully coherent with the matrix. Edwards et al. [9] found that separated Si- and Mg-clusters, and Mg-Si co-clusters exist in the early stage of aging using the atom probe field ion microscope (APFIM) technique. Marioara et al. [15] reported that pre-β″ phase with a composition of $(Al+Mg)_5Si_6$ will be formed before the precipitation of β″. The Al atoms in a pre-β″ phase will be replaced by Mg and Si atoms during annealing. The pre-β″ phase was considered to be the most developed G.P. zone and occurs just before the formation of the β″ phase. Chen et al. [16] claimed that the nano-sized precipitates begin as tiny nuclei with a composition close to $Mg_2Si_2Al_7$ with a Si_2 pillars providing the skeleton for the nano-particles to evolve in the composition. Among all the nucleated second phase particles, the β″ phase has attracted extensive attentions since this precipitate is associated with the peak-aged condition. The β″ precipitate aligning along Al <100> directions and with a needle-like shape was determined to have a composition of Mg_5Si_6 by Andersen et al. [17]. It should be noted that various crystal structures for the β″ precipitate have been proposed [18, 19]. The next phase appearing after the β″ phase is the β′ phase. β′ phase has a rod-like shape and aligns along Al <100> directions, with the hexagonal structure of a=7.05 Å and c=4.05 Å [4]. Matsuda et al. used energy dispersive spectroscopy (EDS) to obtain a Mg:Si ratio of 1.68 for β′ phase [9]. It was recently suggested that β′ phase has an h.c.p. structure with a=7.15 Å and c=12.15 Å and a formula of Mg_9Si_5 [20]. The equilibrium β phase appears at over-aged stages. It has a CaF_2 type f.c.c. structure with a=6.39 Å and appears as platelets along Al {100} planes.

In the present work, the precipitation sequence and the morphology of the precipitates for Al-0.89Mg-0.75Si (in wt.%) alloy with trace Fe and Zn elements at different aging stages were re-investigated using transmission electron microscope

(TEM) and high resolution transmission electron microscope (HRTEM). Hardness test was also performed in order to study the effect of the precipitation sequence on the mechanical behavior of the Al-Mg-Si alloy.

2. Experimental

The chemical composition of the investigated alloy is $Al_{98.255}Mg_{0.89}Si_{0.75}Fe_{0.049}Zn_{0.056}$ (in wt.%). The alloy was prepared in an induction furnace under an argon atmosphere. The as-cast ingot was solution heat-treated at 550 °C for 5h, and subsequently quenched in ice-water. The quenched ingot was then artificial aging treated at 180 °C for various periods of time. The thermal stability of the alloy during aging was analyzed using a NETZSCH STA 449C differential scanning calorimeter (DSC). The sample for DSC testing was equilibrated at 20 °C and then heated to 560 °C with a heating rate of 20 °C per min under an argon atmosphere. The morphologies of the precipitates at different aging stages were studied using transmission electron microscopy (TEM). The TEM specimens were prepared by twin jet electro-polishing in a 30% nitric acid and 70% methanol solution at -26 °C, and examined in Tecnai G^2 20 microscopy and JEOL-3010 high resolution transmission electron microscopy (HRTEM) operated at 200 kV. The hardness of the specimens under all aged stages was measured to obtain the relationship between the mechanical properties and the microstructure of the alloy. Each hardness value is the average value from at least three individual tests.

3. Results and discussion

3.1. Thermal stability

Figure 1 shows the DSC curve of the tested alloy. Two exothermic peaks (B and C) can clearly be observed. Peak B is related to the precipitation of metastable β″ and β′

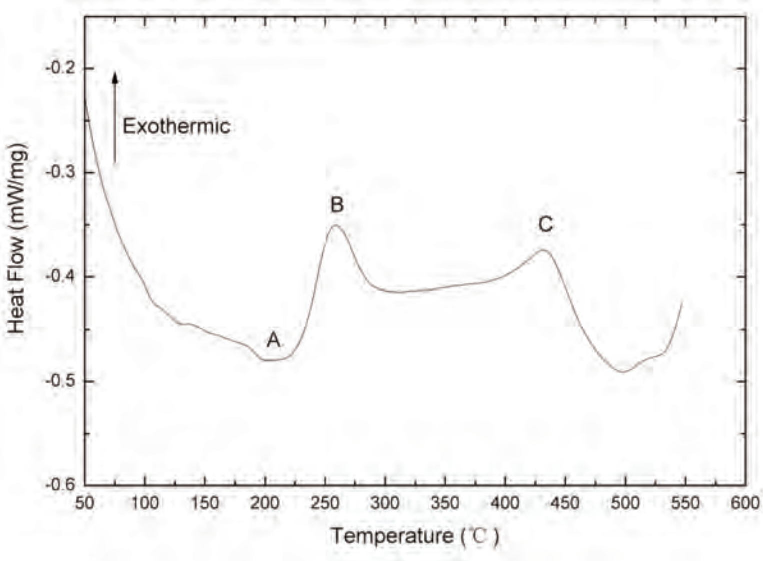

Figure 1: Differential scanning calorimetry curve of the tested Al-Mg-Si alloy (with a heating speed of 20 °C per min).

precipitates, while peak C is related to the precipitation of equilibrium β particles. Previous investigation [21] indicated that when the atomic ratio of Mg to Si is greater than ~1.25, the two exothermic peaks of β'' and β' precipitates overlap to a large one and thus are difficult to be distinguished. The difference between two exothermic peaks of β'' and β' precipitates became more obviously if the Si content increases. In the present work, the atomic ratio of Mg to Si is 1.39, which is larger than the critical value of 1.25. Such a high atomic ratio makes the exothermic peaks of β” and β’ precipitates overlap to a large one. The dissolution trough A is associated with the dissolution of the G.P. zones and clusters that are typically present in T4 tempered alloys [22].

3.2. Microstructural evolution and precipitation sequence

Figure 2 shows a TEM bright-field micrograph and a corresponding HRTEM micrograph of the alloy after being aged for 5 min at 180 °C. According to the fast Fourier transform (FFT) pattern (an inset in Figure 2b), the beam direction was close to <001> zone axis. It is clearly seen that the precipitates in the alloy after being aged for 5 min have a spherical shape with an intensive distribution. The formation of these precipitates is due to the segregation of the solute Mg and Si atoms. HRTEM image indicates that the precipitates are fully coherent with the Al matrix, and the diffraction spots in the FFT pattern only correspond to Al matrix. The crystal structure of the precipitates is the same as that of the Al-matrix because there is no lattice distortion between them. This kind of the precipitates with spherical shape and coherent with the matrix is known as G.P. zones at that stage, similar to previous studies [5, 23]. The size of these round-shaped G.P. zones is about 5 nm in diameter.

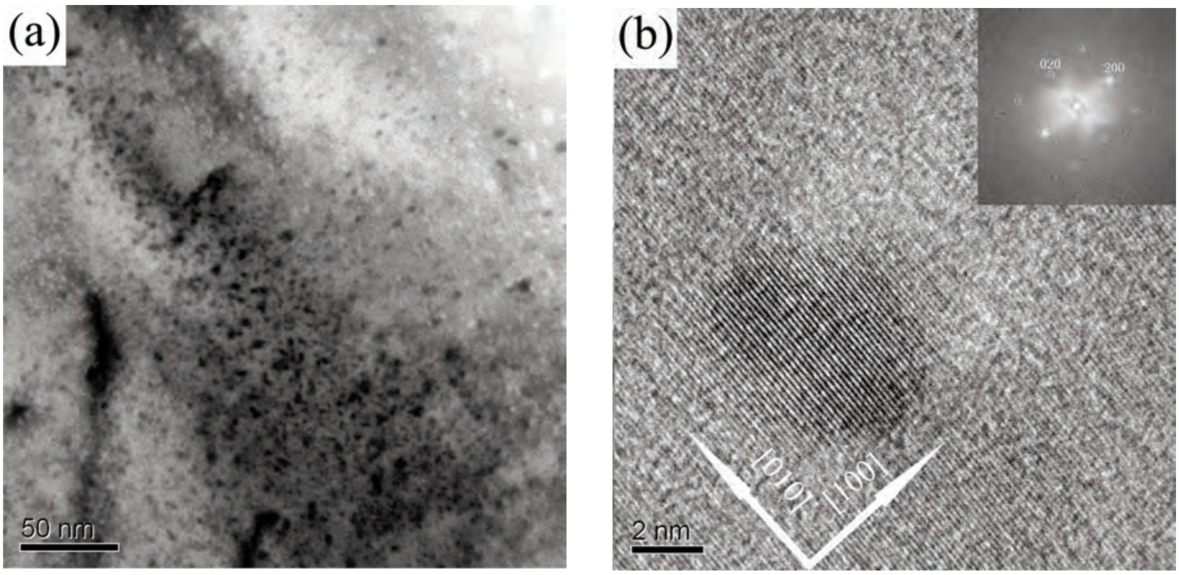

Figure 2. (a) TEM bright field image and (b) HRTEM image of the tested Al-Mg-Si alloy after being aged for 5 min at 180 °C. The electron beam is close to the [001] zone axis.

Figure 3 shows a TEM bright-field micrograph of the alloy after being aged for 1 h at 180 °C. The precipitates have a needle-shaped strain field contrast along <001> directions with some visible dark dots. The needle-like structure shows that the needle direction of the precipitates has the minimum distortion with the matrix so that the precipitates grow along this orientation. It is also indicated that the needle direction of this type of the precipitates is coherent with the matrix. It should be noted that the dark dots are the cross-sections of the needles seen end-on. The edges of these precipitates are clearly visible by the coherency strain field contrast being present in the adjacent Al matrix (position A in Fig. 3). These precipitates are typical β″ phase in Al-Mg-Si alloys. This kind of the semi-coherency structure of the precipitates together with their high number density strongly inhibits dislocation movements and thus increases the yield strength and hardness. The length and mean diameter of the β″ phase are about 50 nm and 4 nm, respectively, suggesting that the β" phase is relatively small.

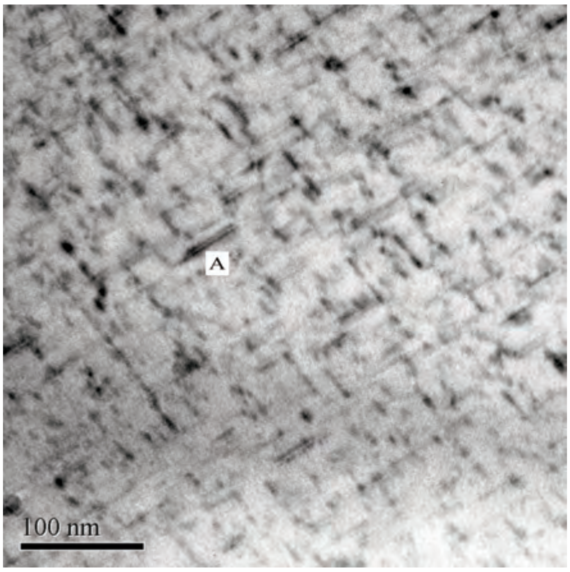

Figure 3. TEM bright field image of the alloy after being aged for 1 h at 180 °C.

Figure 4 shows a TEM bright-field micrograph of the alloy after being aged for 5 h at 180 °C. The morphology of the precipitates has a needle-like shape, similar to the precipitates observed in Figure 3. The precipitates develop their lengths along two directions. Weak streaks, which are pointed by white arrows in Fig.4b, can be observed in the SADP. These streaks originate from the needle-shaped precipitates, which belong to the diffraction pattern of the β″ phase [23, 24]. The length of the β″ phase measured from the graph grows from about 50 nm to about 100 nm, with a few of them being larger than 150 nm, suggesting that the β″ phase has an obvious growth as the aging time increases from 1 h to 5 h. It should be noted that the density of the β″ phase after the alloy being aged for 5 h is higher than that of the specimen after being aged for 1 h.

Figure 5a shows a TEM bright-field micrograph of the specimen after being aged for 10 h at 180 °C. The predominant precipitates at this stage are still β″ particles. However, small numbers of large rod-shaped precipitates, as pointed by black arrows in Fig. 5a, exist in the Al matrix. The length directions of both rod-shaped and needle-shaped precipitates align along Al <100> directions. This particular orientation relationship illustrates that the rod-shaped precipitates are semi-coherent with the matrix.This observation agrees well with some previous studies [3, 4, 20, 25]. The precipitates pointed by white arrows in Fig. 5a can be described as a shorter rod or the cross-sections of the large rod-shaped

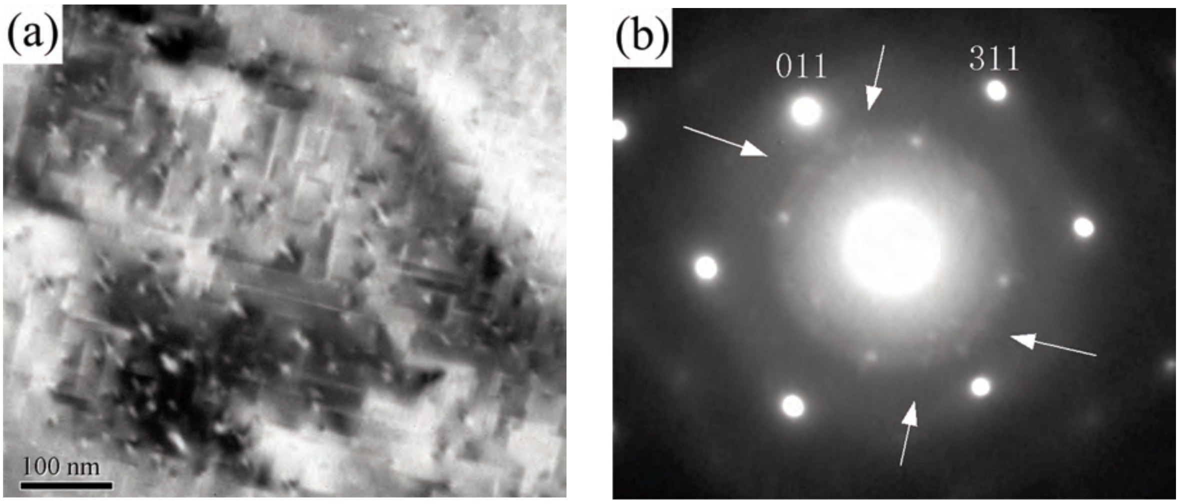

Figure 4. (a) TEM bright field image of the alloy after being aged for 5 h at 180 °C and (b) the corresponding SADP along the Al [$0\bar{1}1$] of the specimen

precipitates. A higher magnification image of the coarse rod phase is shown in Figure 5b. This kind of morphology is different from that of the β″ phase. Although there is a particular orientation relationship between the matrix and the rod direction of the precipitates, the other two directions grow obviously, suggesting that the semi-coherent relationship was destroyed during aging. This type of the rod-shaped morphology is in consistent with the appearance of the β′ precipitates. The length of the β′ phase is in the range of 30-100 nm with a mean diameter of 10-20 nm.

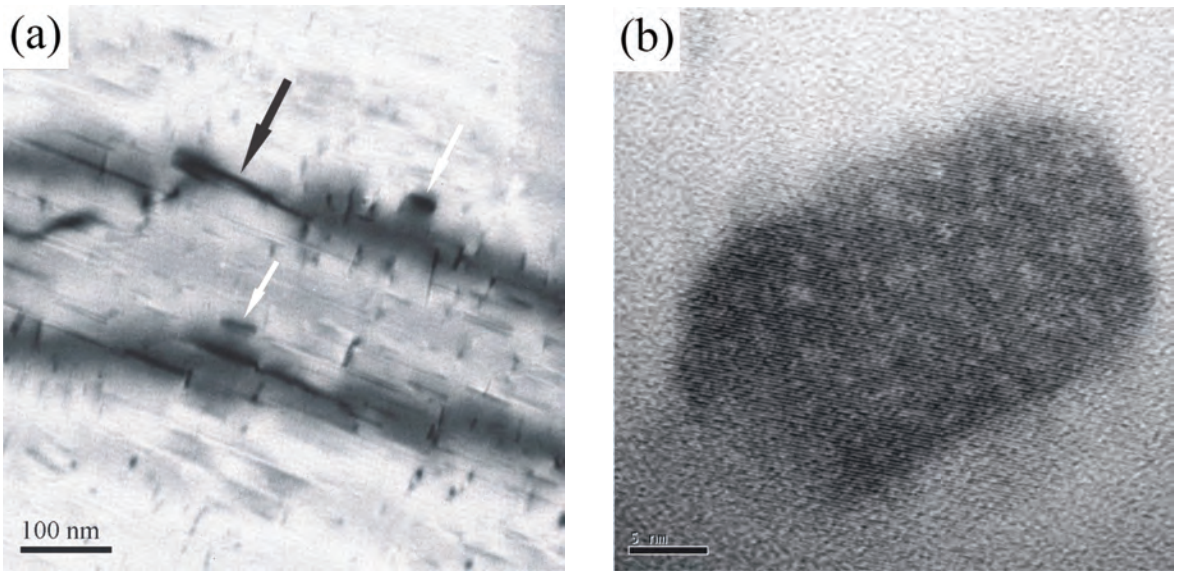

Figure 5. (a) TEM bright field image of the alloy after being aged for 10 h at 180 °C and (b) a HRTEM image of a rod particle.

Figure 6 shows several TEM bright-field micrographs of the specimen after being aged for 30 h at 180 °C, with the zone axis along [011] direction. The rod-shaped precipitates pointed by white arrows in Figures 6a and 6b are the β′ precipitates. It can be seen that the density of the β′ phase increases after being aged from 5 h to 30 h, and the growths in three dimensions happen by comparing the size of the precipitates. Although the precipitate pointed by black arrow in Figure 6a has a similar rod-like morphology, the orientation relationship between the precipitates and the Al matrix is incompatible with the characteristics of β' phase. Previous studies indicated that the plate-shaped plane surface of the equilibrium β phase lays along Al {100} planes [4, 26]. If the observation direction is along the Al <110> directions, an angle will exist between the plane surface of the β phase and the observation direction. Thus, the shape of the platelet β phase may become narrower in the viewing field and present as a rod-shaped morphology. Consequently, this precipitate is identified to be the equilibrium β phase. After being aged at 180 °C for 30h, the metastable precipitates formed via the segregation of Mg and Si atoms precipitate along all directions, destroy the coherent relationship with the matrix, and then transform to the stable β phases. The precipitation process of this phase occurs without fixed orientation relationship with the matrix, and the projection of the β phase appears to be regular plate-shaped morphology. The polygon and rectangular phase pointed by black arrows in Figures 6b and 6c are both equilibrium β phase. Other small irregular shaped precipitates pointed

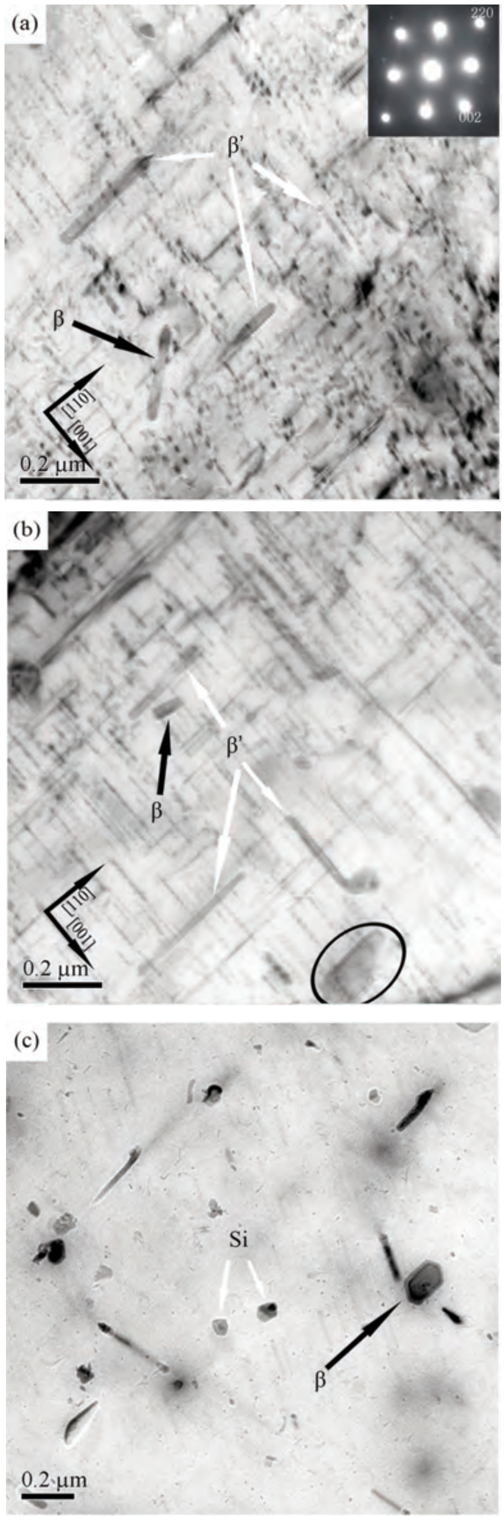

Figure 6: TEM bright field images of the alloy after being aged for 30 h at 180 °C.

by white arrows in Figure 6c are equilibrium Si phase according to EDS analysis. The particle inside the circle of Figure 6b shows how a plate develops from a rod via the growth in a direction normal to the length of the rod. This process is considered to be accompanied by the dissolution of nearby rods. It is noted, however, that the main phase of the alloy after being aged for 30 h at 180 °C is still β″ phase. The strain field contrast of the β″ phase can still be clearly observed in the images, indicating that β″ phase is stable up to 30 hours at this annealing temperature.

In summary, the precipitation sequence of the investigated Al-Mg-Si alloy at 180 °C can be summarized as follows: Al supersaturated solid solution→ G.P. zone → β″ precipitates → β′ precipitates → β precipitates + Si. This precipitation sequence is consistent with the generally accepted precipitation sequence in Al-Mg-Si alloys. The aging time for the presence of different phases is similar to many previous studies [9, 17, 23]. However, some reports showed that β particles are normally difficult to be observed in Al-Mg-Si alloys after being aged for 30 h around 170~180 °C [9, 27], and the duration for the precipitation of β phase is generally longer than 30 hours. The difference might be due to the variation in the composition of the alloys. During aging of some Al-Mg-Si alloys, some other precipitates, such as TPYE-A or U1, were proposed to appear by Matsuda et al. [10] and Andersen et al. [12], respectively. The main difference between our work and the previos studies is due to the variation in aging temperatures. In previous investigations, the aging temperature is about 250 °C or higher, which is higher than the temperature used in our study. In addition, the content of Si in their alloy is also relatively higher. Such a high Si content might induce the nucleation and growth of the TPYE-A or U1 phases during artificial aging treatment.

3.3. Hardness evolution

Figure 7 shows the hardness evolution of the alloy with aging time. The hardness of the alloy was substantially influenced by the aging time. It can be seen that small fluctuations in hardness exist in the very beginning of aging (0~20 min). At that time, the precipitates in the Al matrix are the fully coherent G.P. zones, which have a relatively small contribution to the hardness of the alloy. The hardness of the alloy starts to increase after being aged for about 30 minutes. The hardness reaches its peak value at about 4~6.5 hours, when the needle-shaped β″ precipitates have the maximum density. The hardness starts to decrease with the appearance of the β′ and β precipitates.

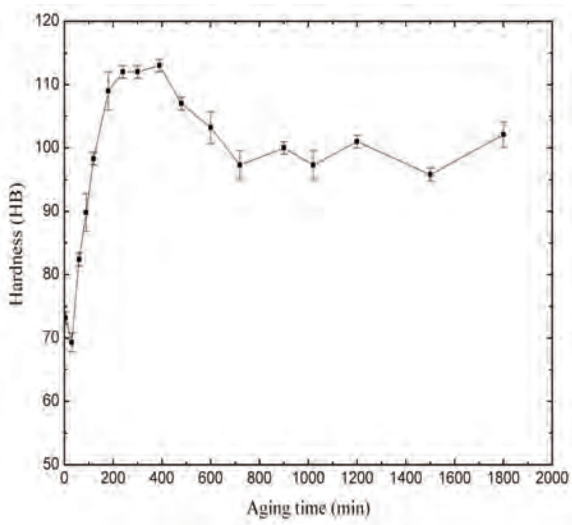

Figure 7: Hardness evolution of the alloy with aging time at 180 °C.

4. Conclusion

Precipitation sequence of an Al-Mg-Si alloy has been investigated by TEM, HRTEM and hardness tests. The results indicate that the precipitation sequence of the Al-0.89 wt.%Mg-0.75 wt. %Si alloy with trace Fe and Zn elements at 180 °C can be summarized as follows: Al supersaturated solid solution→ GP zone → β″ precipitates → β′ precipitates → β precipitates + Si, with the β″ precipitates remaining stable up to 30 hours. The hardness measurements indicate that the main strengthening phase in this Al-Mg-Si alloy is β″ precipitate. The maximum hardness is achieved after 4~6.5 hours of aging time when the alloy has the maximum number density of the β″ precipitates.

Acknowledgement

This work was financially supported by National Natural Science Foundation of China (No. 50831007) and Creative Research Group of National Natural Science Foundation of China (No. 50721003).

References

[1] Y. Du, X. Yuan, W. Sun, B. Hu, J. Mining Metall. B, 45 (2009) 89.

[2] Y. Du, J. Wang, Y.F. Ouyang, L.J. Zhang, Z.H. Yuan, S.H. Liu, P. Nash, J. Mining Metall. B, 46 (2010) 1.

[3] G. Thomas, J. Inst. Met., 90 (1961-62) 57.

[4] M.H. Jacobs, Philos. Mag., 26 (1972) 1.

[5] I. Dutta, S.M. Allen, J. Mater. Sci. Lett., 10 (1991) 323.

[6] N. Maruyama, R. Uemori, N. Hashimoto, M. Saga, M. Kikuchi, Scr. Mater., 36 (1997) 89.

[7] K. Matsuda, Y. Ishida, J. Mater. Sci. 41 (2006) 2605.

[8] K. Matsuda, S. Ikeno, H. Matsui, T. Sato, Mater. Trans. A, 36 (2005) 2007.

[9] G.A. Edwards, K. Stiller, G.L. Dunlop, M.J. Couper, Acta Mater., 46 (1998) 3893.

[10] K. Matsuda, Y. Sakaguchi, Y. Miyata, Y. Uetani, T. Sato, A. Kamia, S. Ikeno, J. Mater. Sci., 35 (2000) 179.

[11] S.J. Andersen, C.D. Marioara, A. Frøseth, R. Vissers, H.W. Zandbergen, Mater. Sci. Eng. A, 390 (2005) 127.

[12] S.J. Andersen, C.D. Marioara, R. Vissers, A. Frøseth, H.W. Zandbergen, Mater. Sci. Eng. A, 444 (2007) 157.

[13] M.A. van Huis, J.H. Chen, H.W. Zandbergen, M.H.F. Sluiter, Acta Mater., 54 (2006) 2945.

[14] M.A. van Huis, J.H. Chen, M.H.F Sluiter, H.W. Zandbergen, Acta Mater., 55 (2007) 2183.

[15] C.D. Marioara, S.J. Andersen, J. Jansen, H.W. Zandbergen, Acta Mater., 49 (2001) 321.

[16] J.H. Chen, E. Costan, M.A. van Huis, Q. Xu, H.W. Zandbergen, Science 312 (2006) 416.

[17] S.J. Andersen, H.W. Zandbergen, J. Jansen, C. Tráhol, U. Tundal, O. Reiso. Acta Mater., 46 (1998) 3283.

[18] N. Maruyama, R. Uemori, N. Hashimoto, M. Saga, M. Kikuchi, Scr. Mater., 36 (1997) 89.

[19] C. Ravi, C. Wolverton, Acta Mater., 52 (2004) 4213.

[20] R. Vissers, M.A. van Huis, J. Jansen, H.W. Zandbergen, C.D. Marioara, S.J. Andersen, Acta

Mater., 55 (2007) 3815.

[21] A. Gaber, N. Afify, M.S. Mostafa, Gh. Abbady, J. Alloys. Compd., 477 (2009) 295.

[22] A.K. Gupta, D.J. Lloyd, S.A. Court, Mater. Sci. Eng. A, 316 (2001) 11.

[23] M. Murayama, K. Hono, Acta Mater., 47 (1999) 1537.

[24] J.P. Lynch, L.M. Brown, M.H. Jacobs, Acta Metall., 30 (1982) 1389.

[25] W.F. Smith, Metall. Trans., 4 (1973) 2435.

[26] K. Matsuda, T. Kawabata, J. Mater. Sci., 37 (2002) 3369.

[27] H.J. Roven, M. Liu, J.C. Werenskiold, Mater. Sci. Eng. A, 483 (2008) 54.